# PERFORMANCE OF OPTIMIZED VLC GSSK SYMBOL SETS IN DISPERSIVE MEDIA

Mandip Shrestha and Deva K. Borah
Klipsch School of Electrical & Computer Engineering
New Mexico State University
Las Cruces, NM 88003, USA
Email: mandip@nmsu.edu, dborah@nmsu.edu

## ABSTRACT

Visible Light Communication (VLC) systems using an array of LEDs as a transmitter and a digital camera as a receiver can provide reliable communication. Such systems can employ various modulation formats that include the generalized space shift keying (GSSK), where only the indices of the LEDs are used to send information. This paper investigates the modeling of GSSK VLC systems under different atmospheric conditions as well as for underwater channels, and investigates the problem of selecting the best set of modulation symbols. The behavior of such systems is modeled using the point spread function, and the inter-symbol Euclidean distance is maximized to obtain the best symbol set. The paper adopts the recently proposed symbol set selection algorithm from the literature exploiting the clustering property of GSSK VLC systems. The results show that the symbol set design algorithm can provide several dBs of gain in the symbol error rate (SER) performance over randomly selected symbol sets in GSSK systems under various atmospheric conditions as well as for underwater channels.

## INTRODUCTION

There are multiple modulation formats that can be used in VLC systems. Examples include the on-off keying (OOK), orthogonal frequency division multiplexing (OFDM), generalized spatial modulation (GSM), spatial modulation (SM) and generalized space shift keying (GSSK) modulation [1] - [3]. Our work in this paper focuses only on the GSSK VLC systems. Such systems have low implementation complexity over SM and GSM systems, where information is present in both LED indices and modulated symbols.

In GSSK systems, each group of transmit bits is mapped to a symbol that actives specific LEDs representing the symbol. Consider a transmitter with an array of $L$ LEDs. If $L_a$ LEDs are activated out of $L$ transmit LEDs, then there are $M_{all} = C(L, L_a)$ possible combinations of transmit LEDs, where $C(n, k) = n!/(n-k)!k!$. For $M$-ary GSSK systems, we need $M$ to be a power-of-two, and the highest possible $M$ is $M = 2^K$ , where $K = \lfloor log_2(M_{all}) \rfloor$ and $\lfloor . \rfloor$ is the floor function. As an example, consider $L$ = 16 and $L_a$ = 3 giving $C(16, 3) = 560$ combinations of transmit LEDs. If the GSSK system is 16-ary, we have to choose the best set of 16 symbols (or combinations) from

$C(560, 16) \approx 3.60 \times 10^{30}$ sets of active LEDs. This is a challenging problem, and algorithms to obtain the best symbol set for GSSK are presented in [4], and extended to GSM systems in [5].
The performance of the algorithm given in [4] has been studied only for indoor systems with no atmospheric effects. Our work here considers outdoor systems including underwater channels. In outdoor systems, the weather may cause poor visibility that makes it hard for an imaging receiver to identify the active LEDs. Weather conditions, such as fog, rain, haze and snow, can cause link failures, and need to be studied. Similarly, in the case of underwater systems, scattering properties of the small particles determine the received signal. Since multiple scattering of light in underwater is a complex process, modeling of VLC systems in underwater channels is a challenging task.
Our study uses the point spread function (PSF) to analyze the communication channel behavior. The PSF gives the system response due to a point source and includes the effect of multiple scattering and attenuation in the medium. Once the PSF is known for a given system, the image due to any light source is obtained using the convolution of the PSF with the original image to get the received image signal under the given weather or underwater conditions.

## SYSTEM MODEL

The transmitter consists of an array of $L$ LEDs arranged in a square of size $\sqrt{L} \times \sqrt{L}$. The received signal $s_l(x, y; x_l, y_l)$ at position $(x, y)$ in the $xy$-plane (i.e., the image plane) due to the $l$-th LED is given by [6]

$$s_l(x, y; x_l, y_l) = A \sum_{i=1}^{\nu} (\frac{\mu}{\mu_0})^2 \frac{e_i}{2\pi\sigma_i^2} \exp(-\frac{(x - x_l)^2 + (y - y_l)^2}{2\sigma_i^2}) \quad (1)$$

where $(x_l, y_l)$ is the image center of the $l$-th LED, $\nu$ is the number of summation terms, $A = 1/p^2$, $p$ is the pixel length, $e_i$ is an LED model parameter, $\sigma_i^2$ is the variance of the $i$-th mixture term, $\mu = f_0/d$ is the image magnification, $f_0$ is the camera focal length, $d$ is the distance between the transmitter and a receiver, $\mu_0$ is the image magnification at a reference distance $d_0$.
Consider the 2-D image at the receiver by the $l$-th LED without any weather or underwater conditions. Let $\mathbf{S}'_l$ be the sample matrix produced by (1). The $(i, j)$-th element of $\mathbf{S}'_l$ is given as $s'_l(i, j; x_l, y_l) = s_l(i\delta_s, j\delta_s; x_l, y_l)$, where $i$ and $j$ are positive integers, and $\delta_s$ is a real number representing the spatial sampling interval along the $x$- and $y$- directions in the image plane. Let $u_l$ define the 'on' or 'off' status of the $l$-th LED. In the presence of a dispersive medium with a PSF $\mathbf{P}$, the received image is modified as $\sum_l (\mathbf{S}'_l * \mathbf{P}) u_l$, where $*$ denotes 2D convolution. The model of the PSF $\mathbf{P}$ is described in the next subsections. The matrix $\mathbf{S}'_l * \mathbf{P}$ for each LED $l$ is rearranged as a column vector by stacking its columns as in [4]. Let $\mathbf{s}_l$ denote this column vector. Define a new matrix $\mathbf{S}$ whose $l$-th column is $\mathbf{s}_l$. The signal vector at the receiver sensor plane is given by

$$\mathbf{r} = \mathbf{Hu} + \mathbf{w} \quad (2)$$

where $\mathbf{H} = \tilde{\mathbf{A}}\mathbf{S}$ is the overall channel matrix, and $\tilde{\mathbf{A}}$ is the pixelization matrix [4]. The vector $\mathbf{u}$ represents a symbol and is of size $L \times 1$. Each element of $\mathbf{u}$ is either a 0 or a 1. The vector $\mathbf{w}$ is a noise vector. Each element $w_m$ of $\mathbf{w}$ is zero-mean Gaussian with a variance $\sigma^2_{w,m} = \alpha\,(\mathbf{Hu} + \mathbf{q}_b)_m + \beta$ , $\alpha$ and $\beta$ are constants, $q_b$ is the background illumination vector. We consider $\sigma^2_{w,m} \approx \sigma^2_w$ for high background illumination.

## POINT SPREAD FUNCTION UNDER ATMOSPHERIC EFFECTS

Light from the transmitter gets scattered in the channel before arriving at the receiver. Although multiple scattering can be neglected in clear air, it is very crucial in weather conditions such as fog or haze. Multiple scattering of light has been studied by many authors. Generally there are two ways to study the scattering of light. One is the Monte-Carlo simulation technique using ray tracing, and the other is the use of the radiative transfer equation (RTE). Monte-Carlo simulation method is too complex computationally when the number of scattering particles is large. RTE method has been extensively studied by the authors in [7]. Generally, two parameters are used to define an atmospheric condition: (1) the optical thickness, $T$, that determines the amount of depletion that a beam of radiation undergoes as it passes through the atmosphere. $T$ is related to the atmospheric visibility $V$ as $T = \sigma d$, where $d$ is the distance between the transmitter and the receiver, and $\sigma = 3.912/V$. The parameter $\sigma$ is called the extinction coefficient. (2) The parameter, $q$, called the forward scattering parameter, whose value is between 0 and 1. The value of $q$ determines the weather conditions as shown in Table 1.

| $q$ | 0.0 - 0.2 | 0.2 - 0.7 | 0.7 - 0.8 | 0.8 - 0.85 | 0.85 - 0.9 | 0.9 - 1 |
|---|---|---|---|---|---|---|
| Weather condition | Air | Aerosols | Haze | Mist | Fog | Rain |

Table 1: Forward scattering parameter and the corresponding weather conditions [8].

PSF for a given atmospheric condition mentioned in [7] is only valid for $T > 1$. The authors in [8] have approximated the PSF in [7] to make it work for every value of $T$ using the modified generalized Gaussian distribution as

$$P_a(x, y; q, T) = \frac{\exp\Big( - \frac{(x^2+y^2)^{\frac{k_1 T}{2}}}{|F(k_1 T, \frac{1-q}{q})|^{k_1 T}} \Big)}{4\Gamma^2(1 + \frac{1}{k_1 T}) F(k_1 T, \frac{1-q}{q})^2} \tag{3}$$

where $F(p, \gamma) = (\frac{\gamma^2 \Gamma(\frac{1}{p})}{\Gamma(\frac{3}{p})})^{\frac{1}{2}}$ is the scale parameter, $\Gamma(.)$ is the Gamma function, i.e., $\Gamma(z) = \int_0^\infty e^{-t} t^{z-1} dt, z > 0$ and $k_1 = 0.5$. The 2D sample matrix produced by (3) in the image plane is $\mathbf{P}$, whose $(i, j)$-th element is given as $P_a(i\delta_s, j\delta_s; q, T)$, where $i$ and $j$ are positive integers.

Figure 1 shows that the value of $T$ determines the shape of the peak of the APSF. As the value of $T$ increases, the shape of the peak becomes broader. Similarly, decreasing the value of $q$ broadens the shape of the PSF as long as the atmosphere is not too thin $(T < 0.3)$. At a very thin atmosphere i.e., higher visibility $(T = 0.1)$ and clean air $(q = 0.1)$, the PSF is almost identical to the delta function. Note that Fig. 1(d) with $T = 0.1$ cannot be obtained using the PSF given in [7]. The cross-sections of the PSF in Fig. 1 indicate that at thick atmosphere $(T > 0.4)$ and under adverse weather conditions for VLC, e.g., haze, fog or rain, the received image of any light source has a glow around it. For pure air $(q < 0.1)$, the visibility is very high so the value of $T$ is always low. For adverse weather conditions, such as haze or fog, the visibility is low so $T$ is always high.

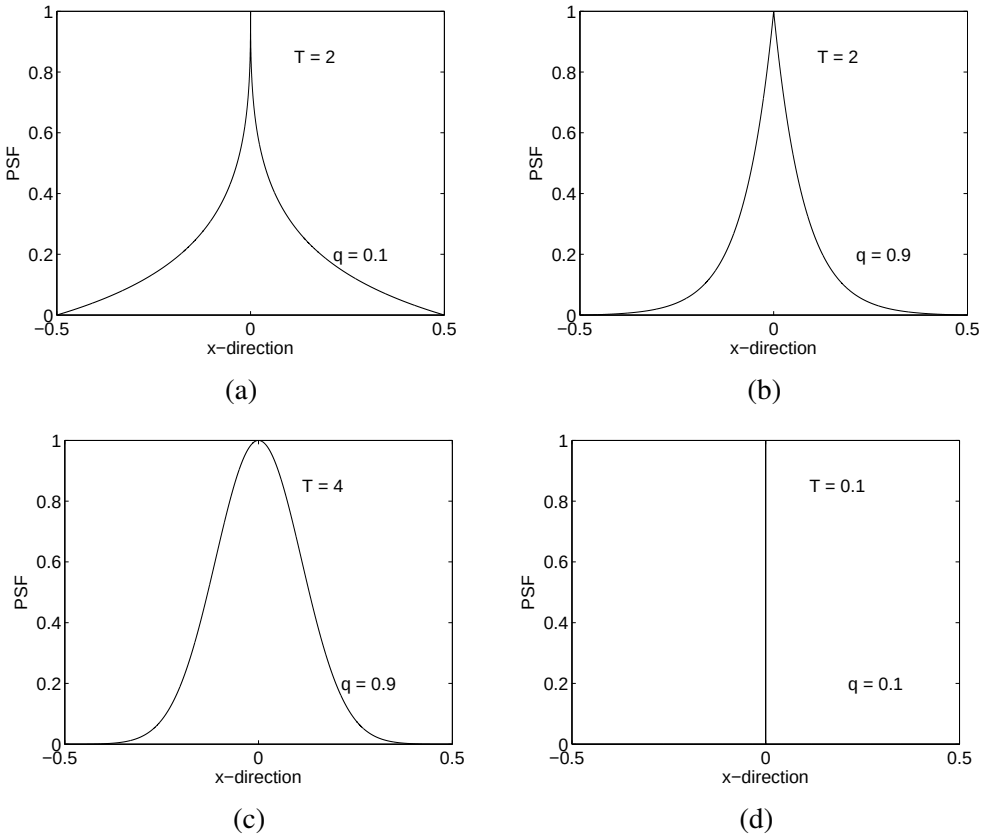


Figure 1: Cross-sections of APSF in different weather conditions

The received image due to foggy weather is shown in Fig. 2. The parameters used are $f_0 = 4.9$ mm, $p$ = 5.5 $\mu$m, $d = 20$ m, $\nu = 2$, $d_0 = 0.1$ m, $e_1$ =5.444$\times 10^{-8}$, $e_2 = 1.126 \times 10^{-6}$, $\sigma_1 = 2.1027 \times 10^{-6}$ m, $\sigma_2 = 3.1392 \times 10^{-6}$ m, $L = 16$, $T = 4$ and $q = 0.9$.

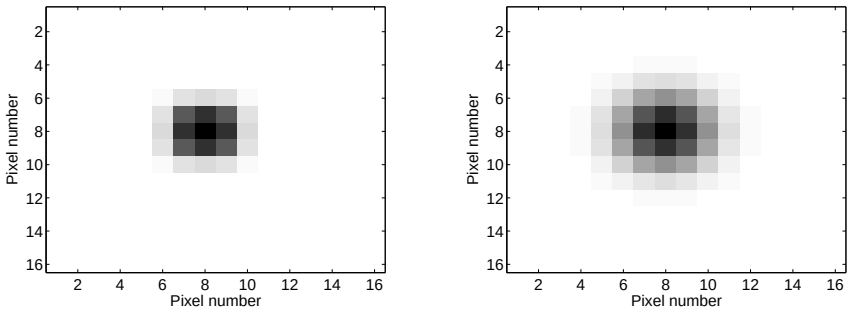


(a) Image without any dispersive media.

(b) Foggy weather image in thick atmosphere.

Figure 2: Signal acquired by the camera receiver due to 16 LEDs at $d$ = 20 m. The darker pixels represent relatively higher intensities.

## POINT SPREAD FUNCTION FOR UNDERWATER CONDITIONS

The scattering and absorption of light cause blurring of images in underwater, thus degrading the performance of VLC systems. Multiple scattering cannot be neglected in underwater communication. This phenomenon has been studied by many authors, and different models of PSF have been given. Using the model given in [9], the PSF for the underwater image is given by

$$
\begin{aligned}
G(\theta_b,\tau_b) &= \frac{\delta(\theta_b)}{\pi\theta_b}e^{-\tau_b} + 0.525\frac{\tau_b}{\theta_b}e^{(-2.6\theta_b^{0.7}-\tau_b)} + \frac{\beta_2^2}{2\pi}[2-(1+\tau_b)e^{-\tau_b}]e^{(-\beta_1(\beta_2\theta_b)^{\frac{1}{3}}-(\beta_2\theta_b)^2+\beta_3)},\\
\beta_1 &= \frac{6.857-1.5737\tau_b+0.143\tau_b^2-6.027\cdot10^{-3}\cdot\tau_b^3+1.069\cdot10^{-4}\cdot\tau_b^4}{1-0.1869\tau_b+1.97\cdot10^{-2}\cdot\tau_b^2-1.317\cdot10^{-3}\cdot\tau_b^3+4.31\cdot10^{-5}\cdot\tau_b^4},\\
\beta_2 &= \frac{0.469-7.41\cdot10^{-2}\tau_b+2.78\cdot10^{-3}\cdot\tau_b^2+9.6\cdot10^{-5}\cdot\tau_b^3}{1-9.16\cdot10^{-2}\cdot\tau_b-6.07\cdot10^{-3}\cdot\tau_b^2+8.33\cdot10^{-4}\cdot\tau_b^3},\\
\beta_3 &= \frac{6.27-0.723\tau_b+5.82\cdot10^{-2}\cdot\tau_b^2}{1-0.072\tau_b+6.3\cdot10^{-3}\cdot\tau_b^2+9.4\cdot10^{-4}\cdot\tau_b^3},
\end{aligned}
\tag{4}
$$

where $\theta_b$ is the scattering angle at which the light is refracted away from its original direction, $\tau_b = \tau\omega$, $\tau$ is the optical length that determines the amount of depletion that a beam of radiation undergoes as it passes through water, and $\omega$ is the single scattering albedo which is the ratio of light scattered to the total light attenuation. The optical length is given by $\tau = \sigma d$, where $\sigma$ is the total attenuation coefficient and $d$ is the distance between the transmitter and the receiver. $\delta$ is related to the direct beam and can be neglected during normalization. For the imaging receiver, we project the PSF $G(\theta_b, \tau_b)$ into the $xy$- plane. For small field angle, first we project PSF in $\theta_b$ to get PSF in $x$- plane using $x = d\theta_b$ and rotate it to get the PSF in $xy$- plane as $P_u(x, y; \omega, \tau)$. We use the sampled version of $P_u$. The $(i, j)$-th element of the sample matrix $\mathbf{P}$ produced by $P_u$ is given as $P_u(i\delta_s, j\delta_s; \omega, \tau)$, where $i$ and $j$ are positive integers.
The received underwater image is shown in Fig. 3. The parameters used are $f_0 = 4.9\,\text{mm}$, pixel width $5.5\,\mu\text{m}$, $d = 10\,\text{m}$, $\nu = 2$, $d_0 = 0.1\,\text{m}$, $e_1 = 5.444 \times 10^{-8}$, $e_2 = 1.126 \times 10^{-6}$, $\sigma_1 = 2.1027 \times 10^{-6}\,\text{m}$, $\sigma_2 = 3.1392 \times 10^{-6}\,\text{m}$, $L = 16$, $\tau = 15$ and $\omega = 0.6$.

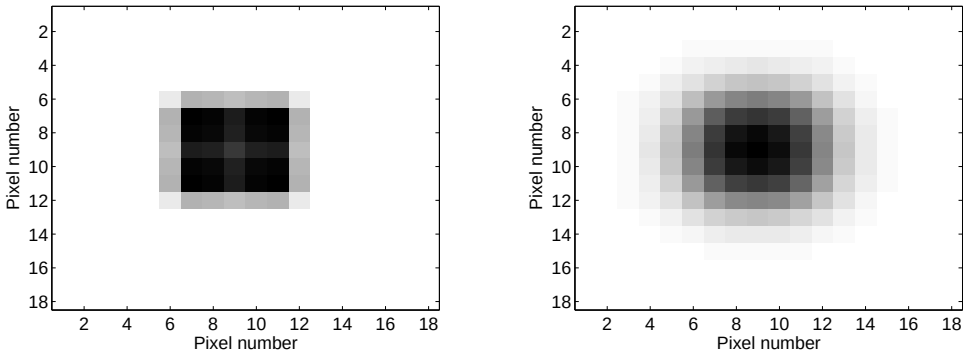


(a) Image without any dispersive media. (b) Image through murky water.

Figure 3: Signal acquired by the camera receiver due to 16 LEDs at $d$ = 10 m. The darker pixels represent relatively higher intensities.

To understand the shape of the PSF, Fig. 4 shows the impact of the values of $\tau$ and $\omega$. As $\tau$ and $\omega$ increase, the shape of the PSF becomes broader. It implies that for pure water (low $\tau$ and $\omega$) the visibility is very high as the shape of the PSF is very thin.

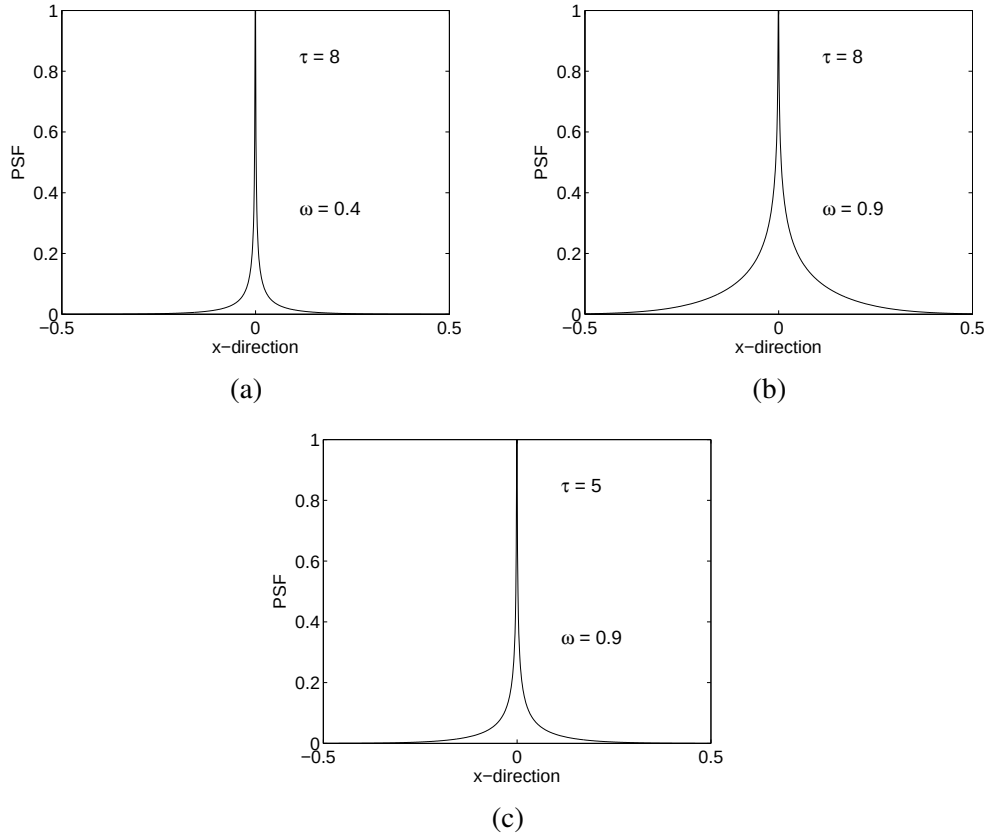


Figure 4: Cross-sections of PSF in different water conditions.

## SYMBOL SET DESIGN

Maximum likelihood (ML) detection is used to detect the active LEDs as

$$\hat{\mathbf{u}} = \arg\min_{\mathbf{u}} || \mathbf{r} - \mathbf{Hu} ||^2 \tag{5}$$

where $\hat{\mathbf{u}}$ is the detected transmit signal vector. The symbol error rate (SER) at the receiver can be approximated as in [4] using the nearest neighbor upper bound,

$$P_e \approx \sum_{i=0}^{i_{max}} \bar{N}_i Q(\frac{D_i}{2\sigma_w}) \tag{6}$$

where $\bar{N}_i$ is the average number of neighbors at Euclidean distance (ED) $D_i$, $D_i = || \mathbf{Hu}_j - \mathbf{Hu}_k ||$ $\forall j, k, j \neq k$ and $Q(x) = 1/\sqrt{2\pi} \int_x^\infty e^{-y^2/2} dy$.

Designing the optimal symbol set is numerically too complex, because an exhaustive search requires searching over $C(M_{all}, M)$ combinations. For VLC systems, the authors in [4] propose to consider only those symbols that involve active LEDs that are close neighbors. We adopt the same algorithm that drastically reduces the search space in finding the best symbol set.

*Step 1:* Consider only those symbols that involve active LEDs located within a cluster radius of $R_c$ from a specific LED, called the cluster center. Each LED can be a cluster center. From each cluster center choose a group of $L_a$ LEDs including the cluster center that are within a distance of $R_c$ from the cluster center. Remove repeated symbols. This reduces the set of total symbols from $M_{all}$ to $M_r$ symbols, where $M_r \ll M_{all}$ usually.

*Step 2:* If $L$ is large, $M_r$ can still be too large, so we need to reduce the set of $M_r$ symbols to a set of $M_s$ symbols so that $M_s < M_r$. We calculate the inter-symbol ED between each pair of symbols in the set containing the $M_r$ symbols. Next, find the minimum value $D_0 = \min_{j,k,j\neq k} || \mathbf{Hu}_j - \mathbf{Hu}_k ||$, and identify the symbols that have the largest number of neighbors at $D_0$ and remove them from the set. Repeat this step until $M_s$ symbols are left.

*Step 3:* This step reduces $M_s$ symbols to $M$ symbols. For this, generate all possible subsets of $M$ symbols from the $M_s$ symbols using a tree structure as given in [4]. For each such subset, compute the inter-symbol distance $D_i$=$D_{jk}$ between each pair of symbols $\mathbf{u}_j$ and $\mathbf{u}_k$ in the subset and the corresponding average number of neighbors. Select the subset that has the largest $D_{min}$ [4].

## NUMERICAL RESULTS

In our numerical results, we use $f_0 = 4.9\,\text{mm}$, $p = 5.5\,\mu\text{m}$, inter-LED distance $\Delta = 1.5$ cm, $\nu = 2$, $d_0 = 0.1\,\text{m}$, $e_1 = 5.444 \times 10^{-8}$, $e_2 = 1.126 \times 10^{-6}$, $\sigma_1 = 2.1027 \times 10^{-6}\,\text{m}$, $\sigma_2 = 3.1392 \times 10^{-6}\,\text{m}$, $L = 16$, $L_a = 2$ and $M = 8$. The signal-to-noise ratio (SNR) is defined as the ratio of electrical power from the averaged intensity received per symbol and the noise variance, $(1/\sigma_w^2)((L_a/L)\sum_{i,j} h_{i,j})^2$ where $h_{i,j}$ is the $(i,j)$-th element of $\mathbf{H}$. Random symbol case uses averaging over 30 randomly selected symbol sets.

Figure 5 shows performance comparison between optimal and randomly selected symbol sets. The analytical and simulation results show accurate match. The optimal symbols using the tree search method provide about 12 dB of gain over randomly selected symbols for the given weather conditions of $T = 1$ and $q = 0.8$. We also show results where the optimal symbol design ignores the knowledge of the $\mathbf{P}$ matrix. We call this as partial channel information (PCI). Optimal symbol set design using PCI has about 7 dB of gain over random symbols case. Locally optimal symbols obtained using a tree search with $M_s = 20$ and $R_c = 1$ give nearly 10 dB of gain.

As the atmosphere becomes thicker, SER performance becomes worse as shown in Fig. 6(a). If the atmospheric density ($T$) is constant with changing weather, the SER performance is better as we move to the right in Table 1 from aerosols to rain which is shown in Fig. 6(b). Higher $q$ value and lower $T$ is expected to give better SER performance at given SNR as long as the atmospheric density is thick ($T > 0.4$) because of decrease in PSF width. SER performance with almost constant gain in the region between the $q$ value of 0.2 and 0.6 in Fig. 6(b) is because it denotes the same weather aerosols in the channel. The drastic change in the SER performance from $q = 0.8$ to $q = 0.9$ is because of change in the weather from a misty to the foggy to the rainy weather.

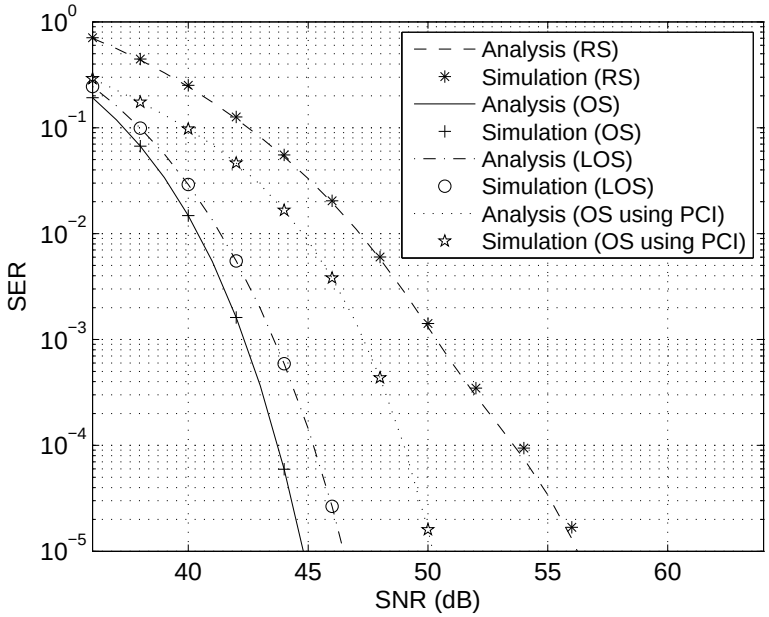


Figure 5: SER performance comparison at misty weather and thick atmosphere defined by $T = 1$ and $q = 0.8$ at a distance of $d = 20\,\text{m}$. 'RS' denotes random symbols, 'OS' denotes optimal symbols and 'LOS' denotes locally optimal symbols. LOS uses $M_s = 20$ and $R_c = 1$.

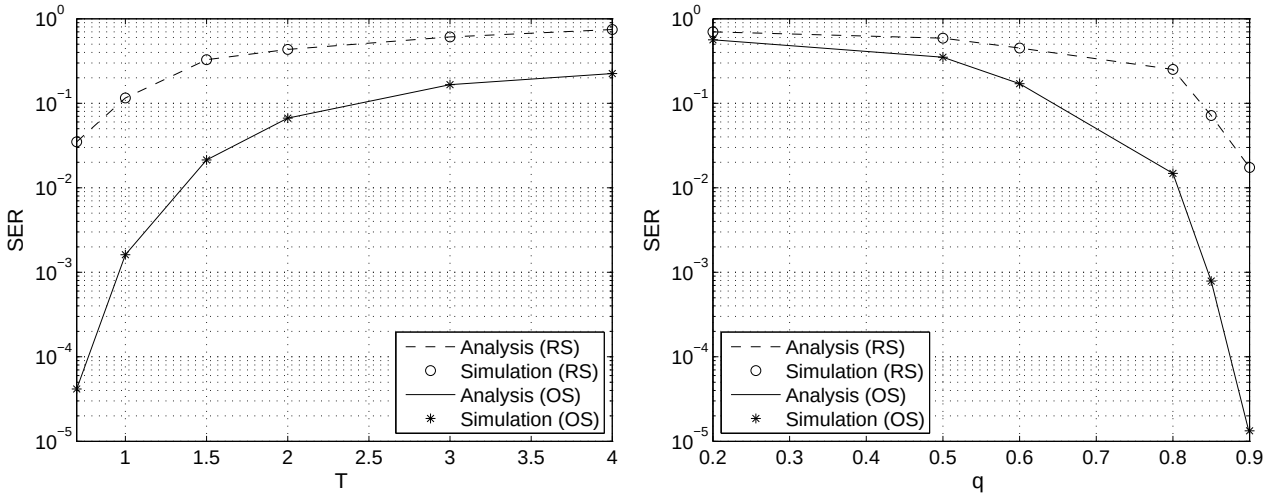


(a) SER vs $T$ keeping $q = 0.8$ and SNR = 42 dB.

(b) SER vs $q$ keeping $T = 1$ and SNR = 40 dB.

Figure 6: SER performance comparison of optimal symbols with randomly selected symbols under different weather conditions at a distance of $d = 20\,\text{m}$. 'RS' denotes random symbols and 'OS' denotes optimal symbols.

In the case of underwater channels, Fig. 7 presents SER performance with the analysis and simulation results for a given water condition. Fig. 7 shows that the optimal symbol using tree search

provides about 11 dB of gain over randomly selected symbols for given water condition of $\tau = 20$ and $\omega = 0.84$. Optimal symbol set design using PCI has about 3 dB gain over random symbol case. The locally searched symbol set with $M_s = 15$ and $R_c = 1$ has about 6 dB gain over randomly selected symbols. As the scattering of light becomes more (i.e., as $\omega$ increases), the SER performance becomes worse as shown in Fig. 8(a). Similarly if attenuation of signal is more (increasing of $\tau$ or $\sigma$) in a given water condition, the SER performance degrades as shown in Fig. 8(b). Lower attenuation of light and less scattering of light improve SER performance at given SNR.

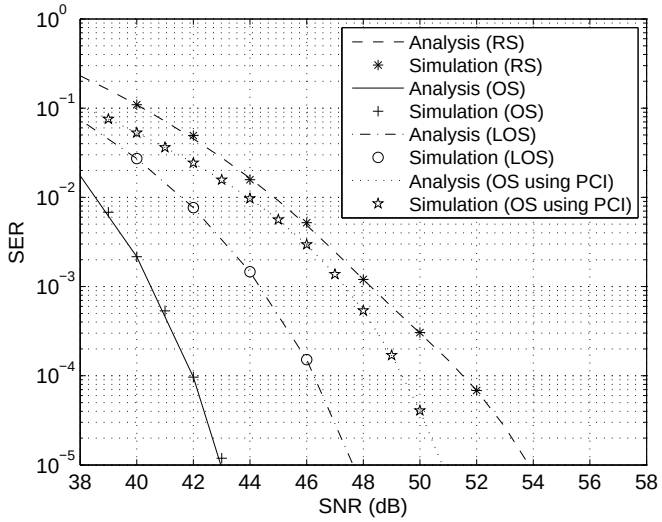


Figure 7: SER performance study for underwater VLC with water conditions given by $\tau = 20$ and $\omega = 0.84$ at a distance of $d = 10\,m$. 'RS' denotes random symbols, 'OS' denotes optimal symbols and 'LOS' denotes locally optimal symbols. LOS uses $M_s = 15$ and $R_c = 1$.

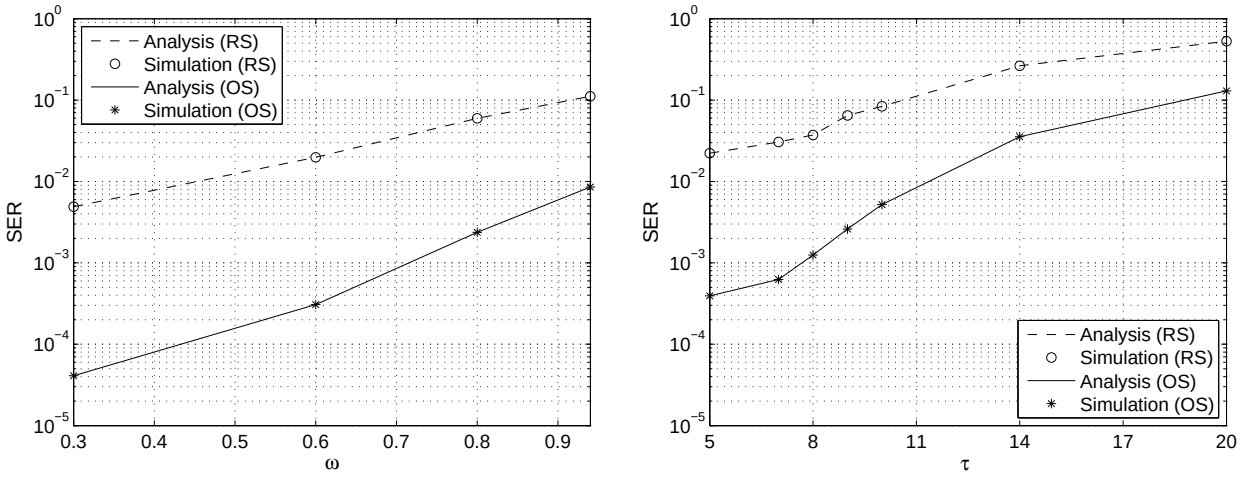


(a) SER versus $\omega$ with $\tau = 9.5$ and SNR = 35 dB. (b) SER versus $\tau$ with $\omega = 0.64$ and SNR = 33 dB.

Figure 8: SER performance comparison for different water conditions at a distance of $d = 10\,$m. 'RS' denotes random symbols and 'OS' denotes optimal symbols.

## CONCLUSIONS

This paper models the GSSK VLC systems for outdoor channels. The effect of the weather and the underwater channel conditions are used to design the optimal symbol sets. For an 8-ary modulated GSSK VLC system, 12 dB SER gain is obtained using the optimal symbol set over randomly selected symbol sets for the weather parameters $T = 1$ and $q = 0.8$ at a distance of $d = 20\,\text{m}$. Similarly, a gain of 11 dB is obtained using the optimal symbol set over randomly selected symbol sets for the water condition described by $\tau = 20$ and $\omega = 0.84$ at a distance of $d = 10\,\text{m}$.

## References


[1] S. P. Alaka, T. L. Narasimhan, and A. Chockalingam, "Generalized Spatial Modulation in Indoor Wireless Visible Light Communication," *Proc. 2015 IEEE Global Communications Conference (GLOBECOM)*, pp. 1–7, San Diego, CA, USA 2015.

[2] P. M. Butala, H. Elgala, and T. D. C. Little, "Performance of optical spatial modulation and spatial multiplexing with imaging receiver," *Proc. 2014 IEEE Wireless Communications and Networking Conference (WCNC)*, pp. 394–399, Istanbul 2014.

[3] W. Popoola, E. Poves, and H. Haas, "Generalised space shift keying for visible light communications," *Proc. 2012 8th International Symposium on Communication Systems, Networks and Digital Signal Processing (CSNDSP)*, pp. 1–4, Poznan 2012.

[4] Y. Sun, D. K. Borah, and E. Curry, "Optimal Symbol Set Selection in GSSK Visible Light Wireless Communication Systems," *IEEE Photonics Technology Letters*, vol. 28, pp. 303–306, Feb. 1 2016.

[5] E. Curry, D. K. Borah, and J. M. Hinojo, "Optimal Symbol Set Design for Generalized Spatial Modulations in MIMO VLC Systems," *Proc. 2016 IEEE Global Communications Conference (GLOBECOM)*, Washington D.C. 2016.

[6] J. Perez-Ramirez and D. K. Borah, "A Single-Input Multiple-Output Optical System for Mobile Communication: Modeling and Validation," *IEEE Photonics Technology Letters*, vol. 26, pp. 368–371, Feb. 15 2014.

[7] S. G. Narasimhan and S. K. Nayar, "Shedding Light on the Weather," *Proc. 2003 IEEE Computer Society Conference on Computer Vision and Pattern Recognition*, vol. 1, pp. 665–672, 2003.

[8] S. Metari and F. Deschenes, "A New Convolution Kernel for Atmospheric Point Spread Function Applied to Computer Vision," *Proc. IEEE 11th International Conference on Computer Vision*, pp. 1–8, Rio de Janeiro 2007.

[9] K. Oliver, W. Hou, and S. Wang, "Image feature detection and matching in underwater conditions," *Ocean Sensing and Monitoring - SPIE 7678*, vol. 2, 2010.